International Journal of Pharmaceutics 624 (2022) 122041

Contents lists available at ScienceDirect

International Journal of Pharmaceutics

journal homepage: www.elsevier.com/locate/ijpharm

Targeting cancer cells in acidosis with conjugates between the carnitine palmitoyltransferase 1 inhibitor etomoxir and pH (low) insertion peptides

Marine Deskeuvre [a,b,1], Junjie Lan [c,1], Emeline Dierge [b], Joris Messens [d,e,f], Olivier Riant [c], Cyril Corbet [b], Olivier Feron [b], Raphaël Frédérick [a,*]

[a] Louvain Drug Research Institute (LDRI), Medicinal Chemistry Research Group (CMFA), Université Catholique de Louvain (UCLouvain), 73 Avenue Emmanuel Mounier, B-1200 Brussel, Belgium
[b] Pole of Pharmacology and Therapeutics (FATH), Institut de Recherche Expérimentale et Clinique (IREC), Université Catholique de Louvain (UCLouvain), 57 Avenue Hippocrate B1.57.04, B-1200 Brussels, Belgium
[c] Institute of Condensed Matter and Nanosciences, MOST Division, Place Louis Pasteur, Université Catholique de Louvain (UCLouvain), Louvain-la-Neuve B-1348, Belgium
[d] VIB-VUB Center for Structural Biology, Vlaams Instituut voor Biotechnologie (VIB), 1050 Brussels, Belgium
[e] Brussels Center for Redox Biology, 1050 Brussels, Belgium
[f] Structural Biology Brussels, Vrije Universiteit Brussel (VUB), 1050 Brussels, Belgium

ARTICLE INFO

Keywords:
pH Low Insertion Peptide
Etomoxir
Conjugates
Cancer
Acidosis
Drug delivery

ABSTRACT

Targeting enzymes involved in tumor metabolism is a promising way to tackle cancer progression. The inhibition of carnitine palmitoyltransferase 1 (CPT1) by etomoxir (Eto) efficiently slows down the growth of various cancers. Unfortunately, the clinical use of this drug was abandoned because of hepatotoxic effects. We report the development of pH-sensitive peptide (pHLIP)-drug conjugate to deliver Eto selectively to cancer cells exposed to acidic microenvironmental conditions. A newly designed sequence for the pHLIP peptide, named pHLIP*d*, was compared with a previously published reference pHLIP peptide, named pHLIP*r*. We showed that the conjugate between pHLIP*d* and Eto has a better pH-dependent insertion and structuration than the pHLIP*r*-based conjugate inside POPC vesicles. We observed antiproliferative effects when applied on acid-adapted cancer cells, reaching a larger inhibitory activity than Eto alone. In conclusion, this study brings the first evidence that pHLIP-based conjugates with a CPT1 inhibitor has the potential to specifically target the tumor acidic compartment and exert anticancer effects while sparing healthy tissues.

1. Introduction

Acidosis, like hypoxia, is a common hallmark of the microenvironment of solid cancers (Corbet and Feron 2017, Pillai, Damaghi et al. 2019). It is now well accepted that acidosis contributes to tumor initiation and progression, as well as to therapy resistance and metastatic dissemination, through several phenotypic alterations including apoptosis evasion, immune surveillance escape, (*epi*)genetic reprogramming, low proliferation/quiescence, epithelial-to-mesenchymal transition and dysregulated metabolism (Peppicelli, Andreucci et al. 2017, Vander Linden and Corbet 2019). In particular, exposure of cancer cells to acidosis leads to profound changes of their metabolic preferences with a shift from glucose to lipid metabolism (Corbet and Feron 2017). Acidic cancer cells actually rely primarily on fatty acid oxidation (FAO) (Corbet, Pinto et al. 2016) as a source of NADPH and acetyl-CoA to fuel the TCA cycle(Carracedo, Cantley et al. 2013). FAO-derived ATP production was further shown to support anoikis resistance and thereby to promote metastatic spreading of acidic cancer cells (Wang, Zeng et al.

Abbreviations: CD, circular dichroism; CM, center of mass; CPT1, carnitine palmitoyltransferase 1; DHA, docosahexaenoic acid; ESI, electrospray ionization; Eto, etomoxir; FA, fatty acids; FAO, fatty acid oxidation; FI_{335}, Fluorescence intensity at 335 nm; HPLC, high-performance liquid chromatography; ITF, intrinsic tryptophan fluorescence; MMA, monomethyl auristatin; MS, mass spectrometry; NMR, nuclear magnetic resonance; pHLIP, pH Low Insertion Peptide; POPC, 1-palmitoyl-2-oleoyl-*sn-glycero*-3-phosphocholine; PSA, polar surface area; PUFA, polyunsaturated fatty acid; SM, spectral maximum; TCA, tricarboxylic acid; TM, transmembrane.

* Corresponding author.
E-mail address: raphael.frederick@uclouvain.be (R. Frédérick).
[1] M.D. and J.L. share the first authorship position.

https://doi.org/10.1016/j.ijpharm.2022.122041
Received 3 March 2022; Received in revised form 7 July 2022; Accepted 18 July 2022
Available online 20 July 2022
0378-5173/© 2022 Elsevier B.V. All rights reserved.

2018, Corbet, Bastien et al. 2020, Sawyer, Qamar et al. 2020). Recently, it was shown that n-3 and n-6 polyunsaturated fatty acid (PUFA) provoke the death of acidic cancer cells, and more complex cell model (*i.e.* spheroid), by ferroptosis (Dierge, Debock et al. 2021). Moreover, n-3 PUFA diet delayed mouse tumor growth when compared with a monounsaturated FA-rich diet.

Carnitine palmitoyltransferase 1 (CPT1) is of particular interest among various enzymes and transporters involved in FA metabolism (Deep and Schlaepfer 2016, Sawyer, Qamar et al. 2020). CPT1 is located in the outer mitochondrial membrane and converts acyl-CoA into acyl-carnitine for transport into the mitochondria. Etomoxir (Eto) is a specific, irreversible, orally available CPT1 inhibitor that can block FAO (Sawyer, Qamar et al. 2020). Studies showed that Eto could slow down tumor progression in ovarian (Sawyer, Qamar et al. 2020), colorectal (Wang, Zeng et al. 2018), prostate cancers (Schlaepfer, Rider et al. 2014). More specifically, Eto was recently reported to prevent distant metastatic spreading of acidosis-exposed colorectal cancer cells (Corbet, Bastien et al. 2020). In a clinical trial for patients suffering from congestive heart failure, hepatotoxicity of Eto was observed (Holubarsch, Rohrbach et al. 2007). Here, we reasoned that the conjugation of this drug to a pH-selective system that would target only cancer cells located in the acidic tumor regions would be of particular interest.

pH Low Insertion Peptides (pHLIP) are pH-responsive peptides derived from the C-helix of a bacteriorhodopsin protein (Andreev, Dupuy et al. 2006). These water-soluble peptides are known to insert across membranes and form a stable transmembrane α-helix upon acidification. At neutral and alkaline pH, the pHLIP is unstructured in solution and monomeric under a concentration of 7 μM (Reshetnyak, Segala et al. 2007) (Fig. 1, state I). However, in the presence of a lipid bilayer, the pHLIP binds to the membrane in a random coil conformation (Fig. 1, state II). In an acidic environment, the transmembrane part (TM) of the peptide folds into an α-helix and inserts across the lipid bilayer (Fig. 1, state III). Upon insertion, the *N*-terminal part of the pHLIP is located in the extracellular medium while its C-terminal part remains inside the cell (Fig. 1, state III). Acidification of the medium eventually triggers the protonation of the aspartate residues present in the TM region of the peptide, thereby enhancing lipophilicity and promoting helical structuration and consecutive insertion across the membrane (Reshetnyak et al., 2006).

pHLIPs have been conjugated to fluorescent dyes through a disulfide bond with the cysteine present at the *N*-terminal flank region (*e.i.* AlexaFluor (Andreev, Dupuy et al. 2007, Reshetnyak, Yao et al. 2011, Weerakkody, Moshnikova et al. 2013, Adochite, Moshnikova et al. 2014, Tapmeier, Moshnikova et al. 2015, Adochite, Moshnikova et al. 2016), Cy5.5 (Andreev, Dupuy et al. 2007, Reshetnyak, Yao et al. 2011, Adochite, Moshnikova et al. 2016), DyLight (Adochite, Moshnikova et al. 2016), IRDye (Adochite, Moshnikova et al. 2014, Adochite, Moshnikova et al. 2016)) for *in vivo* imagine purposes. All the studies demonstrated that these conjugates target primary tumors and even metastatic lesions in mouse models (Reshetnyak, Yao et al. 2011, Adochite, Moshnikova et al. 2014, Adochite, Moshnikova et al. 2016). pHLIPs were also documented to deliver therapeutic agents such as toxins conjugated at the C-terminal flank region (phalloidin (An, Wijesinghe et al. 2010), phallacidin (Wijesinghe, Engelman et al. 2011), amantin (Moshnikova, Moshnikova et al. 2013)), monomethyl auristatins (MMA) (Burns, Robinson et al. 2015, Burns, Hensley et al. 2017), paclitaxel (Onyango, Chung et al. 2015), doxorubicin (Song, Chuan et al. 2016), antimicrobial peptides (AMP)(Burns, McCleerey et al. 2016), peptide nucleic acids (PNA) (Reshetnyak, Andreev et al. 2006, Cheng, Bahal et al. 2015, Svoronos, Bahal et al. 2020). These cargoes are considered non-drug-like due to their high molecular weight (>500 Da) and high polarity (non-favorable logP/log D values) (Svoronos, Bahal et al. 2020). These conjugates have cytotoxic effects on acidic cancer cells and no effects to their neutral homologous cancer cells. Also, they were able to target selectively tumors in mouse models. The pHLIP technology allows the delivery of polar cytotoxic molecules with poor membrane permeability. Recently, Cybrexa therapeutic developed a conjugate, CBX-12, derived from a pHLIP sequence coupled to the topoisomerase I inhibitor exatecan (Gayle, Aiello et al. 2021). Contrary to the above list of cargo drugs, exatecan has a low molecular weight (435.46 g/mol) and a favorable logP value of 1.546. Gayle's team observed a potent *in vivo* cytotoxicity in various human tumor models. They concluded that CBX-12 was applicable to all types of human solid tumors in an antigen-independent manner and a first clinical trial was launched by Cybrexa therapeutics in May 2021.

In the present work, we explore the conjugation of Eto to two pHLIPs, a reference peptide (pHLIP*r*) and a novel pHLIP sequence, pHLIP*d*, designed to potentially improve the tumor-targeting profile. We evaluate the capacity of pHLIP*d* and conjugates to insert in a lipid bilayer using intrinsic tryptophan fluorescence (ITF). Also, we characterized their structuration through circular dichroism spectroscopy (CD). Additionally, we assess the ability of conjugates to reduce tumor proliferation in a 2D acidic cancer cell model sensitized to ferroptosis due to PUFA complementation.

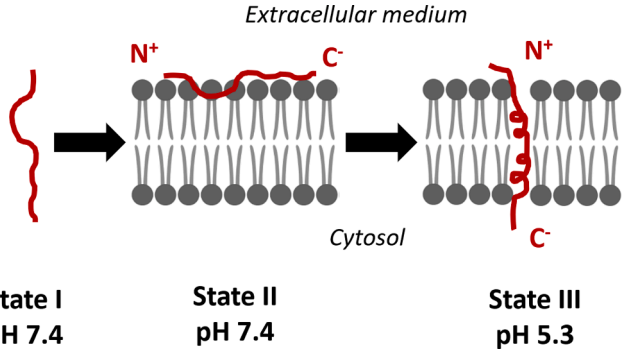


Fig. 1. Schematic representation of the three states of pHLIP. Peptides from the pHLIP family exist in three states: monomeric and unstructured in neutral/basic solution (state I), unstructured and docked on cell membrane at physiological pH (state II), and helical and inserted in the membrane in acidic conditions (state III).

2. Material and methods

2.1. Etomoxir synthesis and modification

2.1.1. General information

Unless otherwise mentioned, reagents were purchased from commercial sources (Merck, TCI, Acros, FluoroChem) and used without further purification. All solvents were dried from Na or CaH_2 and purified by distillation before being used. NMR spectra were recorded at room temperature on a Bruker Avance UltraShield instrument operating at a frequency of 300 MHz for ^{1}H and 75 MHz for ^{13}C. Chemical shifts (δ) are reported in ppm relative to $CDCl_3$ ($\delta = 7.26$ ppm) for ^{1}H NMR and $CDCl_3$ ($\delta = 77.2$ ppm) for ^{13}C NMR multiplicity (s = singlet, d = doublet, t = triplet, q = quartet, m = multiplet). Column chromatography was performed over ROCC Silica gel 60 (40–63 μm). Thin layer chromatography was performed on prepared thin layers precoated plates: Silica gel Merck 60 F254. The visualization of spots on TLC plates was done by UV light (254 nm or 365 nm) or $KMnO_4$ solution staining. Mass spectra were recorded using an orbitrap Q Exactive Thermo Fisher spectrometer, a hybrid quadrupole-orbitrap mass spectrometer. ^{1}H NMR, ^{13}C NMR and HRMS analysis of compound **10** and **14** are shown in Supporting information section (**Fig. S1-S6**).

2.1.2. 6-bromohexan-1-ol **(2)** (CAS: 4286–55-9)

To a solution of hexane-1,6-diol **1** (10.00 g, 84.62 mol) in Tol (100 mL), HBr (aq. 48 % in water, 9.57 mL, 84.62 mol) was added dropwise at room temperature. The mixture was stirred and heated at reflux for 18 h. TLC analysis indicated that substantial amounts of hexane-1,6-diol

remained. Thus, a further quantity of HBr (2.00 mL) was added, and the mixture was heated at reflux for 6 h, at which time TLC monitoring showed complete conversion. The reaction mixture was cooled to room temperature, and the organic layer was separated. Then, the organic layer was diluted with Et_2O and washed with 1 M NaOH and brine, dried over anhydrous $MgSO_4$, filtered and concentrated *in vacuo* to give a yellow oil. The crude was purified by silica gel column chromatography (PE/EtOAc: 5/1) to give the compound 6-bromohexan-1-ol **2** as a colorless oil (13.89 g, 90%).

Chemical Formula: $C_6H_{13}BrO$, **Molecular weight:** 181.07 g/mol.

HRMS ESI: Calculated for $C_6H_{12}Br$ $[M-OH]^-$: 163.0117, found: 163.0114.

^{1}H NMR (300 MHz, $CDCl_3$, δ ppm): 3.64 (t, $J = 6.0$ Hz, 2H), 3.40 (t, $J = 9.0$ Hz, 2H), 2.09–2.00 (m, 1H), 1.93–1.80 (m, 2H), 1.62–1.53 (m, 2H), 1.49–1.35 (m, 4H).

*2.1.3. 1-((6-bromohexyl)oxy)-4-chlorobenzene **(4)** (CAS: 37136–99-5)*

The 1-((6-bromohexyl)oxy)-4-chlorobenzene **4** was prepared following a procedure previously reported by *D. Gärtner et al.* (2015). To a solution of triphenylphosphine (7.10 g, 27.06 mmol), 6-bromohexan-1-ol **2** (5.00 g, 27.06 mmol), and 4-chlorophenol **3** (3.48 g, 27.06 mmol,) in dry THF (30 mL) was added at 0 °C diisopropyl azodicarboxylate (DIAD) (6.24 mL, 29.77 mmol, 94% purity) dropwise. After the addition, the reaction mixture was stirred for 18 h at room temperature. After concentration under *vacuo,* the residue was diluted with Et_2O and washed with water and brine, dried over anhydrous $MgSO_4$, filtered and concentrated *in vacuo* to give a yellow oil. The crude was purified by silica gel column chromatography (PE/EtOAc: 20/1) to give the compound 1-((6-bromohexyl)oxy)-4-chlorobenzene **4** as a colorless oil (6.69 g, 85%).

Chemical Formula: $C_{12}H_{16}BrClO$, **Molecular weight:** 291.61 g/mol.

HRMS ESI: Calculated for $C_{12}H_{17}BrClO$ $[M+H]^+$: 291.0146, found: 291.0146.

^{1}H NMR (300 MHz, $CDCl_3$, δ ppm): 7.22 (d, $J = 9.0$ Hz, 2H), 6.81 (d, $J = 9.0$ Hz, 2H), 3.92 (t, $J = 6.0$ Hz, 2H), 3.44 (t, $J = 6.0$ Hz, 2H), 1.94–1.74 (m, 4H), 1.56–1.48 (m, 4H).

^{13}C NMR (75 MHz, $CDCl_3$, δ ppm): 157.67, 129.29 (2C), 125.37, 115.75 (2C), 68.03, 33.81, 32.67, 29.03, 27.92, 25.28.

*2.1.4. Diethyl 2-(6-(4-chlorophenoxy)hexyl)malonate **(6)** (CAS: 82258–39-7)*

The diethyl 2-(6-(4-chlorophenoxy)hexyl)malonate **6** was prepared following a procedure previously reported by *G. Kang et al.* (2018). Sodium malonate was obtained by adding NaH (760 mg, 60% NaH in mineral oil, 18.86 mmol) in portions to a solution of dimethyl malonate **5** (3.18 mL, 18.86 mmol) in THF (40 mL) at 0 °C. The resulting suspension was stirred for 0.5 h. The 1-((6-bromohexyl)oxy)-4-chlorobenzene **4** (5.0 g, 17.15 mmol) was then added in the mixture at room temperature. After completion of the reaction monitored by TLC (around 4 h), the solvent was removed under reduced pressure. The residue was dissolved with saturated aqueous NH_4Cl and extracted two times with DCM. The organic extracts were combined and washed with water and brine, dried over anhydrous $MgSO_4$, filtered and concentrated *in vacuo* to give a brownish yellow oil. The crude was purified by silica gel column chromatography (PE/EtOAc: 20/1–10/1) to give the compound diethyl 2-(6-(4-chlorophenoxy)hexyl)malonate **6** as a light yellow oil (3.89 g, 61%).

Chemical Formula: $C_{19}H_{27}ClO_5$, **Molecular weight:** 370.87 g/mol.

HRMS ESI: Calculated for $C_{19}H_{28}ClO_5$ $[M+H]^+$: 371.1620, found: 371.1620.

^{1}H NMR (300 MHz, $CDCl_3$, δ ppm): 7.23 (d, $J = 9.0$ Hz, 2H), 6.82 (d, $J = 9.0$ Hz, 2H), 4.22 (q, $J = 9.0$ Hz, 4H), 3.92 (t, $J = 6.0$ Hz, 2H), 3.33 (t, $J = 6.0$ Hz, 1H), 1.96–1.88 (m, 2H), 1.80–1.75 (m, 2H), 1.40–1.32 (m, 6H), 1.28 (t, $J = 6.0$ Hz, 6H).

^{13}C NMR (75 MHz, $CDCl_3$, δ ppm): 169.52 (2C), 157.67, 129.24 (2C), 125.30, 115.73 (2C), 68.15, 61.29, 61.00, 53.42, 52.03, 29.05, 28.96, 28.64, 27.23, 25.73, 14.10.

*2.1.5. 8-(4-chlorophenoxy)-2-(ethoxycarbonyl)octanoic acid **(7)** (CAS: 82258–38-6)*

The diethyl 2-(6-(4-chlorophenoxy)hexyl)malonate **6** (3.00 g, 8.09 mmol) was added to a solution of KOH (455 mg, 8.09 mmol) in EtOH (20 mL) at room temperature. After 18 h of stirring, the solvent was removed under reduced pressure. The residue was dissolved in 1 M HCl and extracted three times with EtOAc. The organic extracts were combined and washed with water and brine, dried over anhydrous $MgSO_4$, filtered and concentrated *in vacuo* to give the crude product. The residue was purified by silica gel column chromatography (DCM/MeOH v/v 50/1 0.5% AcOH) to give the compound 8-(4-chlorophenoxy)-2-(ethoxycarbonyl)octanoic acid **7** as a light yellow solid (2.30 g, 83%).

Chemical Formula: $C_{17}H_{23}ClO_5$, **Molecular weight:** 342.82 g/mol.

^{1}H NMR (300 MHz, $CDCl_3$, δ ppm): 7.21 (d, $J = 9.0$ Hz, 2H), 6.80 (d, $J = 9.0$ Hz, 2H), 4.20 (q, $J = 9.0$ Hz, 4H), 3.90 (t, $J = 6.0$ Hz, 2H), 3.38 (t, $J = 6.0$ Hz, 1H), 1.94–1.92 (m, 2H), 1.80–1.71 (m, 2H), 1.48–1.38 (m, 6H), 1.28 (t, $J = 6.0$ Hz, 3H).

^{13}C NMR (75 MHz, $CDCl_3$, δ ppm): 174.77, 169.49, 157.65, 129.24 (2C), 125.32, 115.73 (2C), 68.12, 61.74, 51.57, 29.03, 28.91, 28.82, 27.13, 25.70, 14.05.

*2.1.6. Ethyl 8-(4-chlorophenoxy)-2-methyleneoctanoate **(8)** (CAS: 82258–37-5)*

To a solution of 8-(4-chlorophenoxy)-2-(ethoxycarbonyl)octanoic acid **7** (4.00 g, 11.67 mmol) in DCM (20 mL) was added diethylamine (1.24 mL, 11.67 mmol) and paraformaldehyde (550 mg, 17.50 mmol) at 0 °C, then the mixture was heated to reflux for 18 h. The reaction mixture was cooled to room temperature, diluted with more DCM and washed with 10% aqueous citric acid solution and brine, dried over anhydrous $MgSO_4$, filtered and concentrated *in vacuo* to give the crude product. The residue was purified by silica gel column chromatography (PE/EtOAc: 10/1) to give the compound ethyl 8-(4-chlorophenoxy)-2-methyleneoctanoate **8** as a yellow oil (2.78 g, 76%).

Chemical Formula: $C_{17}H_{23}ClO_3$, **Molecular weight:** 310.82 g/mol.

^{1}H NMR (300 MHz, $CDCl_3$, δ ppm): 7.19 (d, $J = 9.0$ Hz, 2H) 6.78 (d, $J = 9.0$ Hz, 2H), 6.12 (d, $J = 3.0$ Hz, 1H), 5.49 (d, $J = 3.0$ Hz, 1H), 4.18 (q, $J = 9.0$ Hz, 2H), 3.87 (t, $J = 6.0$ Hz, 2H), 2.32–2.27 (m, 2H), 1.77–1.70 (m, 2H), 1.51–1.33 (m, 6H), 1.28 (t, $J = 6.0$ Hz, 3H).

^{13}C NMR (75 MHz, $CDCl_3$, δ ppm): 167.24, 157.72, 140.96, 129.21 (2C), 125.23, 124.24, 115.72 (2C), 68.15, 60.51, 31.78, 29.10, 28.91, 28.33, 25.79, 14.21.

*2.1.7. Ethyl 2-(6-(4-chlorophenoxy)hexyl)oxirane-2-carboxylate **(9)** (CAS: 82258–36-4)*

To a solution of ethyl 8-(4-chlorophenoxy)-2-methyleneoctanoate **8** (2.00 g, 6.43 mmol) in 1,2-DCE (25 mL) was added *m*-CPBA (4.33 g, 19.30 mmol, 77%) at 0 °C, then the mixture was heated to reflux 18 h. The reaction mixture was cooled to room temperature and diluted with DCM. After pH adjustment to 8 with saturated aqueous $NaHCO_3$, the mixture was extracted with DCM twice. The organic layers were combined and washed with water and brine, dried over anhydrous $MgSO_4$, filtered and concentrated *in vacuo* to give a brownness oil. The oil was purified by silica gel column chromatography (PE/EtOAc: 20/1–10/1) to give the compound ethyl 2-(6-(4-chlorophenoxy)hexyl)oxirane-2-carboxylate **9** as a light yellow oil (1.33 g, 63%).

Chemical Formula: $C_{17}H_{23}ClO_4$, **Molecular weight:** 326.82 g/mol.

HRMS ESI: Calculated for $C_{17}H_{23}ClO_4Na$ $[M+Na]^+$: 349.1177, found: 349.1176.

^{1}H NMR (300 MHz, $CDCl_3$, δ ppm): 7.23 (d, $J = 9.0$ Hz, 2H), 6.82 (d, $J = 9.0$ Hz, 2H), 4.32–4.14 (m, 2H), 3.92 (t, $J = 9.0$ Hz, 2H), 3.04 (d, $J = 6.0$ Hz, 1H), 2.79 (d, $J = 6.0$ Hz, 1H), 2.15–2.06 (m, 2H), 1.83–1.73 (m, 2H), 1.51–1.37 (m, 6H), 1.30 (t, $J = 6.0$ Hz, 3H).

^{13}C NMR (75 MHz, $CDCl_3$, δ ppm): 170.40, 157.68, 129.24 (2C),

125.30, 115.73 (2C), 68.15, 61.58, 57.00, 51.83, 31.17, 29.22, 29.03, 25.81, 24.71, 14.12.

*2.1.8. 2-(6-(4-chlorophenoxy)hexyl)oxirane-2-carboxylic acid **(10)** (CAS: 124151–60-6)*

The ethyl 2-(6-(4-chlorophenoxy)hexyl)oxirane-2-carboxylate **9** (2.00 g, 6.12 mmol) was added to a solution of KOH (360 mg, 6.43 mmol) in aqueous EtOH (20 mL, EtOH/H_2O: 9/1) for 15 h at room temperature. The solvent was removed under reduced pressure, and the resulting residue was dissolved in 1 M HCl and extracted three times with EtOAc. The combined organic layers were washed with water and brine, dried over anhydrous $MgSO_4$, filtered and concentrated *in vacuo* to give a yellow crude product. The residue was purified by silica gel column chromatography (DCM/MeOH: 50/1) to give the compound 2-(6-(4-chlorophenoxy)hexyl)oxirane-2-carboxylic acid **10** as a yellow solid (1.60 g, 88%).

Chemical Formula: $C_{15}H_{19}ClO_4$, **Molecular weight:** 298.76 g/mol.

HRMS APCI: Calculated for $C_{15}H_{19}ClO_4Na$ $[M+Na]^+$: 321.0861, found: 321.0864.

^{1}H NMR (300 MHz, $CDCl_3$, δ ppm): 10.13 (s, 1H), 7.21(d, J = 9.0 Hz, 2H), 6.80 (d, J = 9.0 Hz, 2H), 3.90 (t, J = 9.0 Hz, 2H), 3.08 (d, J = 6.0 Hz, 1H), 2.87 (d, J = 6.0 Hz, 1H), 2.19–2.13 (m, 1H), 1.79–1.69 (m, 2H), 1.67–1.66 (m, 1H), 1.60–1.40 (m, 6H).

^{13}C NMR (75 MHz, $CDCl_3$, δ ppm): 174.24, 157.65, 129.25 (2C), 125.32, 115.73 (2C), 68.11, 57.18, 52.25, 30.52, 29.16, 29.01, 25.79, 24.59.

*2.1.9. (2-hydroxyethyl)pyridyl disulfide **(13)** (CAS: 111625–28-6)*

The (2-hydroxyethyl)pyridyl disulfide **13** was prepared following a procedure previously reported by *R. Horikawa et al.* (2016). To a solution of 2,2′-Dipyridyldisulfide **11** (2.00 g, 8.90 mmol) in MeOH (20 mL) supplemented with AcOH (0.5 mL) was added a solution of 2-mercaptoethanol **12** (460 μL, 4.45 mmol) in MeOH (5 mL) dropwise over a 30 min period under continuous stirring at room temperature. The reaction mixture was further stirred for 18 h at room temperature. Then, the solvent was removed under reduced pressure to give a yellow oil. The crude was purified by silica gel column chromatography (PE/EtOAc: 10/1) to give the compound (2-hydroxyethyl)pyridyl disulfide **13** as light yellow oil (748 mg, 78%).

Chemical Formula: $C_7H_9NOS_2$, **Molecular weight:** 187.28 g/mol.

HRMS ESI: Calculated for $C_7H_{10}NOS_2$ $[M+H]^+$: 188.0198, found: 188.0199.

^{1}H NMR (300 MHz, $CDCl_3$, δ ppm): 8.51–8.49 (m, 1H), 7.61–7.55 (m, 1H), 7.41–7.38 (m, 1H), 7.17–7.12 (m, 1H), 5.74 (s, 1H), 3.80 (t, J = 9.0 Hz, 2H), 2.95 (t, J = 4.0 Hz, 2H).

^{13}C NMR (75 MHz, $CDCl_3$, δ ppm): 159.13, 149.79, 136.89, 121.82, 121.49, 58.30, 42.59.

*2.1.10. 2-(pyridin-2-yldisulfaneyl)ethyl-2-(6-(4-chlorophenoxy)hexyl) oxirane-2-carboxylate **(14)***

To a solution of 2-(6-(4-chlorophenoxy)hexyl)oxirane-2-carboxylic acid **10** (200 mg, 0.670 mmol) in DCM (10 mL) was added DMAP (25 mg, 0.200 mmol), (2-hydroxyethyl)pyridyl disulfide **13** (131 mg, 0.736 mmol), EDCI (193 mg, 1.00 mmol), HOBt (136 mg, 1.00 mmol) and DIPEA (166 μL, 1.00 mmol). The mixture was stirred for 18 h at room temperature. After, the mixture was diluted with DCM and washed with water and brine, dried over anhydrous $MgSO_4$, filtered and concentrated in *vacuo* to give a yellow oil. The crude was purified by silica gel column chromatography (PE/EtOAc: 10/1) to give the compound 2-(pyridin-2-yldisulfaneyl)ethyl 2-(6-(4-chlorophenoxy)hexyl)oxirane-2-carboxylate **14** as a yellow oil (224 mg, 71%).

Chemical Formula: $C_{22}H_{26}ClNO_4S_2$, **Molecular weight:** 468.02 g/mol.

HRMS ESI: Calculated for $C_{22}H_{27}ClNO_4S_2$ $[M+H]^+$: 468.1065, found: 468.1065.

^{1}H NMR (300 MHz, $CDCl_3$, δ ppm): 8.46–8.43 (m, 1H), 7.65–7.61 (m, 2H), 7.18 (dd, J = 3.0, 9.0 Hz, 2H), 7.10–7.05 (m, 1H), 6.78 (dd, J = 9.0 Hz, 2H), 4.48–4.31 (m, 2H), 3.88 (t, J = 6.0 Hz, 2H), 3.06–3.02 (m, 3H), 2.77 (d, J = 6.0 Hz, 1H), 2.10–2.02 (m, 1H), 1.76–1.59 (m, 3H), 1.52–1.35 (m, 6H).

^{13}C NMR (75 MHz, $CDCl_3$, δ ppm): 169.96, 159.09, 157.39, 149.56, 136.85, 129.00 (2C), 125.01, 120.77, 119.71, 115.50 (2C), 67.92, 62.83, 56.72, 51.75, 36.80, 30.89, 28.93, 25.63, 24.51.

2.2. Peptide synthesis and conjugation with etomoxir

pHLIP*d*, K-pHLIP*d*, pHLIP*r*, and K-pHLIP*r* were synthesized and purified by Genecust or Proteogenic firm. Compound **14** and peptide were dissolved in a mixture of water and acetonitrile (1/1). The reaction medium was agitated for 18 h at room temperature. Analytical HPLC-MS determined the formation of conjugate (Agilent Zorbax Eclipse 5 μm × 4.6 × 50 mm; flow rate 1 mL/min phase A: water 0.1%TFA; phase B acetonitrile 0.1% TFA; gradient: 15 min 95/5 A/B to 20/80 A/B) and conjugates were purified through semi-preparative high pressure liquid chromatography (Phenomenex Kinetex 5 μm × 150 × 21.2 mm; flow rate 25 mL/min phase A: water 0.1% TFA; phase B acetonitrile 0.1% TFA) or Sep pack column. After sample lyophilization, the purity was checked by analytical HPLC-MS (purity < 95% for all conjugates, see SI Fig. S7-14).

Name	Sequence	Calculated $(M+3H^+)^{3+}$	Found $(M+3H^+)^{3+}$
pHLIP*d*-Eto (**15**)	AADDQNPWRAYLDLLFPTDTLLLDLLVDADEGTC(-S-S-$(CH_2)_2$-etomoxir)G	1541.45	1402.75
K-pHLIP*d*-Eto (**17**)	AADDQNPWRAYLKLLFPTKTLLLKLLVDADEGTC(-S-S-$(CH_2)_2$-etomoxir)G	1541.45	1416.40
pHLIP*r*-Eto (**16**)	AAEQNPIYWARYADWLFTTPLLLLDLALLVDADEGTC(-S-S-$(CH_2)_2$-etomoxir)G	1541.45	1533.35
K-pHLIP*r*-Eto (**18**)	AAEQNPIYWARYAKWLFTTPLLLLKLALLVDADEGTC(-S-S-$(CH_2)_2$-etomoxir)G	1541.45	1541.70

2.3. Preparation of POPC vesicles

Unilamellar vesicles of 100 nm diameter were prepared from 1-palmitoyl-2-oleoyl-*sn-glycero*-3-phosphocholine (POPC) supplied by Merck. 700 μL of 25 mg/mL POPC in chloroform were evaporated (40 °C, 450 atm, 2 h). The dried lipid film was rehydrated with 1 mL of 5 mM NaPi pH 8.0 and mixed by vigorous vortex for 30 s. The resulting multilamellar vesicles solution was frozen in a bath of dry ice in acetone (-78 °C) and then reheated to 55 °C in a water bath for five cycles. Then, the liposomes were extruded through a polycarbonate membrane with 100 nm diameter pores using a mini extruder (Avanti Polar Lipids) to produce large unilamellar vesicles. Lipid concentration was checked using the SPV reaction (Anschau, Caruso et al. 2017). The size distribution was monitored by dynamic light scattering analysis performed at a scattering angle of 173° using zeta sizer Nano ZS from Malvern instruments.

2.4. Circular dichroism (CD) spectroscopy

First, a lyophilized stock of peptide or conjugate was dissolved in 5 mM sodium phosphate pH 8.0. Then, peptide concentration was controlled by Eppendorf BioSpectrometer using the extinction coefficient ε_{280} = 6990 $M^{-1}cm^{-1}$ or 13890 $M^{-1}cm^{-1}$ in function of studied

pHLIP. Afterwards, peptides were incubated with POPC vesicles (prepared as described earlier) in 5 mM NaPi pH 8.0 buffer. Finally, the pH was adjusted with 0.1 M sodium phosphate and sodium fluoride pH 5.0 buffer or 0.1 M sodium phosphate and sodium fluoride pH 8.0 buffer (60 µL). The pH value was checked with a micro-pH-meter. The final sample volume was 600 µL. The lipid/peptide was 200:1 with a final peptide concentration around 8 to 10 µM. Measurements were performed on Jasco J-715 spectropolarimeter at 25 °C. Spectra were collected from 195 to 260 nm in 1 nm steps. Each spectrum was corrected with the corresponding blank spectrum, sample without peptide.

2.5. Intrinsic tryptophan fluorescence measurements

Peptide dissolved in 5 mM sodium phosphate pH 8.0 was incubated during 1 h in the presence of liposomes (prepared as described earlier) in the same ratio as the CD experiment for 1 h. Then, the mixture was transferred to a 96 wells-plate (187.5 µL). The pH of the well was adjusted with 0.1 M sodium phosphate and sodium fluoride buffer (62.5 µL) to obtain the desired pH values. The final peptide concentration was 3.75 µM. The mixture was incubated 30 min before the measurement. Emission spectra were recorded using a SpectraMax M2 spectrophotometer from Molecular Devices. The excitation wavelength was 280 nm, and the emission wavelength range was 310 to 400 nm with a step of 1 nm. Liposomes blanks were subtracted for peptide samples, whereas lipid blanks with the drug at the same concentration for conjugates. Center of mass (CM), spectra maximal (SM), and fluorescence intensity at 335 nm (FI_{335}) were used to determine the pKa. CM was calculated following this formula: $CM = \sum_1^n I_{i\lambda_i} / \sum_1^n I_i$ Where I_i is the fluorescence intensity measured at a wavelength λ_i.

2.6. Cell culture

Hypopharyngeal FaDu cancer cell line was purchased from ATCC. Cell lines were stored according to the supplier's instructions and used within 6 months after resuscitation of frozen aliquots. All cells were maintained in DMEM supplemented with 10% heat-inactivated FBS, 10 mM D-glucose, 2 mM L-glutamine and 25 mM of PIPES and HEPES before adjusting the pH to 7.4 or 6.5. Acid-adapted cancer cells were established as previously described (Corbet, Draoui et al. 2014). All cell lines were tested for mycoplasma contamination with the MycoAlert™ Mycoplasma Detection kit (Lonza). Cell density was determined by using the Presto Blue reagent (Thermo Fisher Scientific) according to manufacturer's instructions. After collection, cell number was assessed by cell counting on a hemocytometer with Trypan Blue exclusion dye.

2.6.1. 2D culture cell

Each treatment was performed in a full culture medium with 10 µM CPT1 inhibitor etomoxir. Cell growth medium was supplemented with 100 µM BSA-conjugated fatty acids for 72 h. Docosahexaenoic acid (10–2206/DHA) was purchased from Larodan. DHA was conjugated with BSA in PBS as to obtain a fatty acid/BSA ratio of 4:1 (w:w).

3. Results

3.1. Design of sequence variants of pHLIP by mutating the flanks

We designed a sequence of pHLIP to optimize drug delivery to acidic cancer cells. In their pioneering publication in 2013, the team of Engelman and Reshtnyak reported 16 different pHLIP variants derived from WT-pHLIP (Table 1) (Weerakkody, Moshnikova et al. 2013). These pHLIPs were fully characterized for their insertion capabilities into a lipid bilayer model. Among the most promising variants, the variant number 3 (Table 1, Var3) coupled with a fluorophore displayed the highest tumor-targeting activity in a murine model. However, its C-terminal part is truncated compared to WT-pHLIP; thus, limiting its use as a drug carrier. A negative control was designed for Var3 corresponding to the same sequence in which aspartic acids were replaced by lysine (Table 1, K-Var3). This sequence failed to reveal a pH-dependent interaction of the peptide with the lipid bilayer and to target the acidic compartment of mouse tumors.

Table 1
Structures of pHLIP investigated. All presented sequences start with the *N*-terminal part on the left and the underlined residues correspond to the transmembrane region. The Engelman and Reshtnyak team's optimized the wild-type pHLIP (WT-pHLIP) to obtain a fluorescent conjugate presenting the highest tumor/organ ratio, named variant 3 (Var3). The team also reported the negative control of Var3 in which the aspartic acids presented in the transmembrane part were replaced by lysine (K-Var-3). The referenced pHLIP (pHLIP*r*) is a reported peptide used as a cargo delivery tool (An, Wijesinghe et al. 2010) Considering Var3 and pHLIP*r* sequences, we designed a new peptide sequence, named pHLIP*d*. K-pHLIP*d* and K-pHLIP*r* correspond to negative control of each respective pHLIP*d*/*r*.

Name	Sequence
WT-pHLIP	AC<u>EQNPIYWARYADWLFTTPLLLLDLALLV</u>DADEGT
Var3	AC<u>DDQNPWRAYLDLLFPTDTLLLDLLW</u>
K-Var3	AC<u>DDQNPWRAYL*K*LLFPT*K*TLLL*K*LLW</u>
pHLIP*r*	AAEQNPIY<u>WARYADWLFTTPLLLLDLALLV</u>DADEGT*C*G
pHLIP*d*	AADDQNP<u>WRAYLDLLFPTDTLLLDLLV</u>DADEGT*C*G
K-pHLIP*d*	AADDQNP<u>WRAYL*K*LLFPT*K*TLLL*K*LLV</u>DADEGT*C*G
K-pHLIP*r*	AAEQNPIY<u>WARYA*K*WLFTTPLLLL*K*LALLV</u>DADEGT*C*G

Since the goal of this study is to deliver Eto inside cancer cells, we also investigated the sequences that were employed to transport cargoes. The published sequences were very similar to each other except from some minor mutations (Onyango, Chung et al. 2015, Burns, McCleerey et al. 2016, Song, Chuan et al. 2016, Burns, Hensley et al. 2017). Thus, we replaced the *N*-terminal cysteine of Var 3 with an alanine considering the sequence of a referenced peptide (Table 1, pHLIP*r*) (An, Wijesinghe et al. 2010). The pHLIP*r* sequence is derived from WT-pHLIP after replacing *N*-terminal cysteine with alanine and adding cysteine and glycine in the C-terminal part (Adochite, Moshnikova et al. 2014, Tapmeier, Moshnikova et al. 2015, Adochite, Moshnikova et al. 2016). Moreover, we modified the last residue of Var3 in favor of a valine considering the sequences of pHLIPs conjugated to peptidic or chemical cargoes (Onyango, Chung et al. 2015, Burns, McCleerey et al. 2016, Song, Chuan et al. 2016, Burns, Hensley et al. 2017). After this final consideration, we obtained the designed pHLIP, pHLIP*d*, depicted in Table 1.

3.2. Etomoxir synthesis, modification, and conjugation to peptide

The carboxylic acid analog of etomoxir (compound **10** Fig. 2) was prepared according to an original seven-step strategy (Fig. 2). First, the intermediate **6** was obtained through bromination of the diol **1**, followed by Mitsunobu reaction (Gartner, Stein et al. 2015) with the phenol **3** and a nucleophilic substitution reaction with diethyl malonate **5** (Kang, Yamagami et al. 2018). A controlled saponification of diester **6** was achieved to obtain the monoester **7**, which on treatment with paraformaldehyde and diethylamine yielded the unsaturated ester **8**. The ethyl oxirane carboxylate **9** was then acquired by oxidation of the compound **8** with 3-chloroperoxybenzoic acid. Finally, the ester **9** was hydrolyzed under mild conditions to get the target molecule **10**. Thus, we obtained the compound **10** in an overall yield of 16% in 7 steps from starting diol **1**. We also checked the Log P (3.9), log $D_{7.4}$ (0.6) and PSA (59.1 $Å^2$) of molecule **10** with Chemicalize calculator from ChemAxon. There are to our knowledge no other cargoes conjugated to pHLIP that present a log P higher than 1.546 (*i.e.* exatecan) (Svoronos, Bahal et al. 2020).

In the literature, drugs are generally conjugated to pHLIPs via a disulfide bond with the cysteine present at the C-terminal part (Onyango, Chung et al. 2015, Song, Chuan et al. 2016, Burns, Hensley et al. 2017).

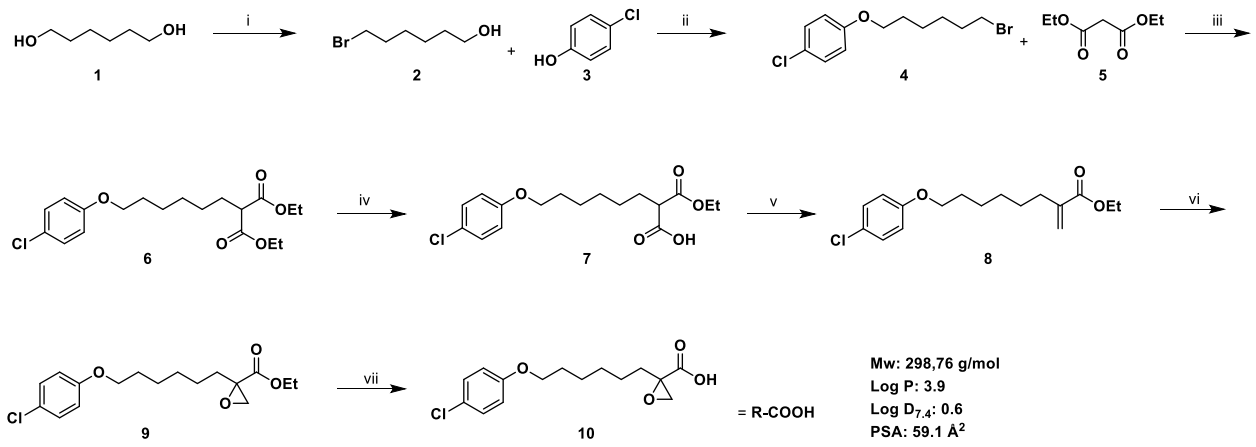


Fig. 2. Synthetic route for Etomoxir acid version. (i) HBr 48% (1.0 eq), Tol, reflux, 24 h, 90%; (ii) **3** (1.0 eq), Ph_3P (1.0 eq), DIAD (1.1 eq), THF, 0 °C → r.t., 18 h, 85%; (iii) **5** (1.1 eq), NaH (60% in mineral oil, 1.1 eq), THF, 0 °C → r.t., 4.5 h, 61%; (iv) KOH (1.0 eq), EtOH, r.t., 18 h, 83%; (v) $NHEt_2$ (1.0 eq), paraformaldehyde (1.5 eq), DCM, 45 °C, 18 h, 76%; (vi) *m*-CPBA (3.0 eq), 1,2-DCE, 0 °C → 85 °C, 18 h, 63%; (vii) KOH (1.05 eq), EtOH/H_2O (v/v 9/1), r.t., 88%. LogP and PSA values were calculated from Chemicalize chemical properties calculator (ChemAxon).

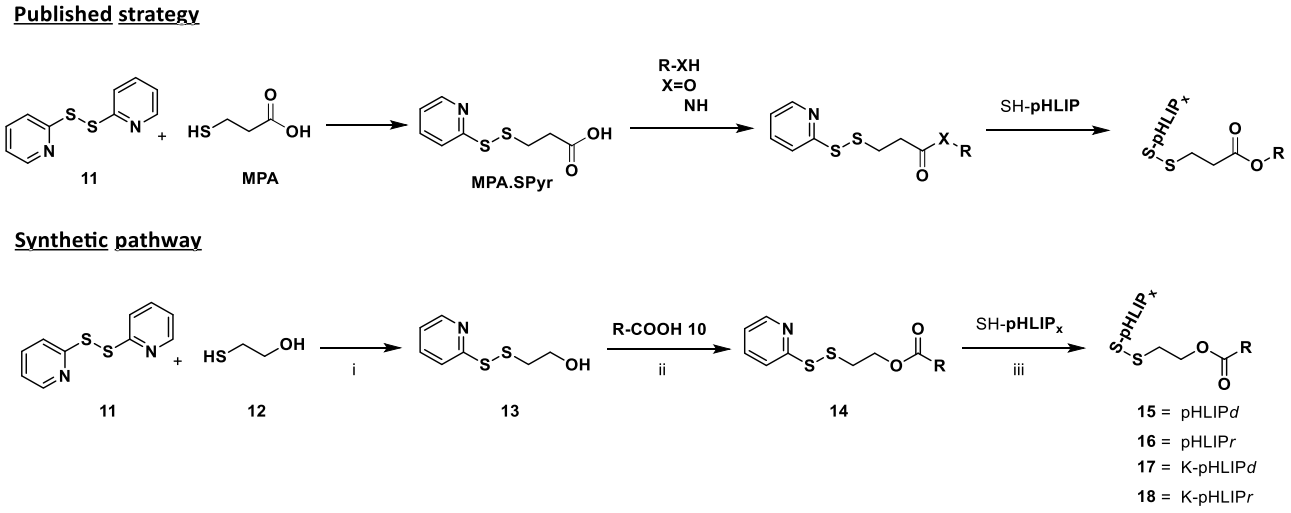


Fig. 3. Synthetic route for conjugates. (i) **12** (0.5 eq), AcOH (1.0 eq), MeOH, r.t., 18 h, 78 %; (ii) **13** (1.1 eq) DMAP (0.3 eq), HOBt (1.5 eq), EDCI (1.5 eq), DIPEA (1.5 eq), DCM, r.t., 18 h, 71 %; (iii) SH-**pHLIPx** (1.0 eq) ACN/H_2O (v/v 1/1), r.t., 18 h, **15** 44%, **16** 35%, **17** 44 %, **18** 49%.

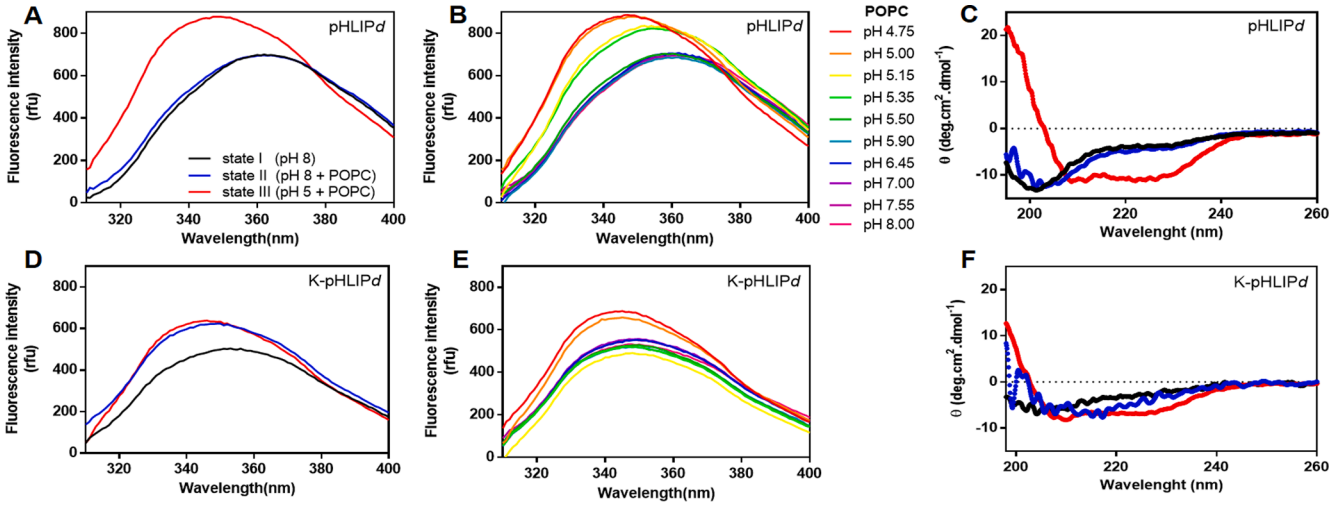


Fig. 4. Interactions of designed peptide (pHLIP*d*) and its negative control (K-pHLIP*d*) with lipid bilayers. Tryptophan fluorescence measurements (**A, B, D, E**) and CD spectroscopy (**C, F**) of peptides in state I (pH 8), state II (pH 8 and POPC vesicles), and state III (pH 5 and POPC vesicles). pHLIP*d* presents a pH-dependent insertion (**A, B**) and structuration (**C**) inside the POPC vesicles, while K-pHLIP*d* shows no preference of insertion and structuration at various pH conditions (**D, E, F**).

The published strategy (Fig. 3) consists of a disulfide exchange between 2,2′-dithiopyridine (**11**) and mercaptopropionic acid (MPA) to form 3-(2-pyridinyldithio)propanoic acid (MPA.SPyr). Then, the intermediate before the peptide coupling was obtained by condensation of an amine or a hydroxyl group of the drugs with MPA.SPyr. Based on this strategy, the disulfide-alcohol **13** was synthesized after a reaction between two equivalents of the disulfide **11** and 2-mercaptoethanol **12**. The etomoxir ester **14** was obtained from compounds **13** and **10** by esterification using *N*-ethyl-*N'*-(3-dimethylaminopropyl)carbodiimide hydrochloride (EDCI) as a coupling agent (Horikawa, Sunayama et al. 2016). Finally, the conjugates (Fig. 3 (**15**–**18**)) between the modified inhibitor and the peptides ((K)-pHLIP*d/r*) were synthesized in a mixture of acetonitrile and water (1/1) and then purified by semi-preparative high performance liquid chromatography (HPLC) system.

3.3. Biophysical characterization of the pHLIP's

To validate its pH-dependent insertion capability, we characterized the newly designed pHLIP*d* by intrinsic tryptophan fluorescence (ITF). First, we incubated pHLIP*d* with POPC vesicles at pH 8 for 1 h. Following this incubation, peptides were adsorbed on the liposome surface corresponding to state II (Fig. 1). Afterward, we incubated the resulting mixture in buffers at pH 5 and pH 8 for 30 min. We also prepared a solution without liposomes in a buffer solution at pH 8 to mimic state I (Fig. 1). When pHLIP*d* was exposed to water molecules in alkaline buffer, the tryptophan fluorescence intensity was low, and its spectral maximum was around 360 nm (Fig. 4 **A**, state I/ black curve). A similar observation was made for peptides in the presence of POPC vesicles (Fig. 4 **A**, state II/ blue curve). However, in an acidic buffer solution at pH 5, we observed gain of fluorescence intensity and a maximum spectral shift around 340 nm, confirming the peptide insertion inside the vesicles (Fig. 4 **A**, state III/ red curve). Acidic pH correlates with an increase of the peptide fluorescence due to peptide insertion inside the POPC vesicles. ITF experiments with buffer solutions at different pH (Fig. 4 **B**) led to the evaluation of the *pKa* of pHLIP*d*, corresponding to the pH value where 50% of the peptide is inserted in POPC vesicles while the other 50% is in solution. We monitored this value following three parameters: the maximal spectral (SM) intensity, the center of mass (CM), and the fluorescence intensity at 335 nm (FI_{335}) (Scott, Westerfield et al. 2017). An SM parameter of 4.95 (Table 2), consistent with the one published for Var3 (5.06), was found (Weerakkody, Moshnikova et al. 2013).

To characterize the conformational change undergone by pHLIP*d*, we used circular dichroism (CD), a spectroscopic technique that allows to determine secondary structures in proteins. We studied the peptide in the same conditions as for the fluorescence measurements. The data revealed a minimum of ellipticity around 200 nm for the state I (Fig. 4 **C**, black curve) and state II (Fig. 4 **C**, blue curve) indicating a random coil conformation. Two minima at 210 nm and 220 nm for state III (Fig. 4 **C**, red curve), representing an α-helical structure were observed. The experiment thus confirmed that pHLIP*d* could structure itself in a pH-dependent manner.

As a control, we designed K-pHLIP*d* (Table 2), in which lysine residues were replaced by aspartic acid residues at the pHLIP*d* TM region. This peptide failed to interact with POPC vesicles in a pH-dependent manner. Indeed, no changes in fluorescence intensities and maxima in acidic and neutral pH in the presence of liposomes (Fig. 4 **D, E**) were detected. Additionally, we did not observe the random coil conformation for the state II condition (Fig. 4 **F**, pH 8 + POPC vesicles/ blue curve).

Then, we compared pHLIP*r* and K-pHLIP*r* (Table 1) with pHLIP*d*. A tryptophan fluorescence experiment revealed insertion of pHLIP*r* inside POPC vesicles in a pH-dependent manner as its fluorescence intensity increased with acidity (Fig. 5 **A, B**). At the same time, we did not observe this behavior for its negative control as there was no change of the fluorescence intensities (Fig. 5 **D, E**). For pHLIP*r*, the experimental *pKa* values were higher than those obtained for pHLIP*d* (values in Table 2) and correspond to published ones (Scott, Westerfield et al. 2017). This result indicates that pHLIP*d* has less tendency to insert in the lipid bilayer than pHLIP*r* at a given pH. Interestingly, pHLIP*r* exhibits a structuration into a 3_{10} helix, defined by two minima at 207 nm and 225 nm, in the presence of liposomes in basic conditions according to CD (Fig. 5 **C**, blue curve). These data suggest that pHLIP*r* is partially structured in state II, implying that this peptide presents a higher affinity than pHLIP*d* for cancer cells at physiological pH (7.4). Furthermore, the CD spectra overlay of state II pHLIP*d* (Fig. 5 **F**, dark blue curve) and state II pHLIP*r* (Fig. 5 **F**, light blue curve) confirms the random coil conformation adopted by pHLIP*d* in these conditions.

Next, we examined whether the conjugates could undergo transmembrane insertion with ITF and CD. From these experiments, we observed the insertion and structuration inside POPC vesicles of pHLIP*d*-Eto in a pH-dependent manner. Indeed, the fluorescence intensities were correlated to the pH (Fig. 6 **A, E**) while only acidic medium led to the α-helix formation (Fig. 6 **I**). Meanwhile, no pH dependency is observed in fluorescence study for the insertion of pHLIP*r*-Eto (Fig. 6 **C, G**) although CD spectra revealed a gain in ellipticity from state II to state III (Fig. 6 **K**), supported by the values of the ratio of ellipticity at 222 and 208 nm (state II: 0.80 and state III: 1.13). Both negative controls presented less pH-dependent insertion than the corresponding conjugates regarding the tryptophan fluorescence measurement (Fig. 6 **B, D, F, G**). We did not observe a signal corresponding to α-helix in CD spectra but aggregation of K-pHLIPs (Fig. 6 **J, L**). The tendency of K-pHLIPs to aggregate was previously reported by the team of *Engelman* and *Reshtnyak* (Weerakkody, Moshnikova et al. 2013). The *pKa* of conjugate presenting a pH-dependent insertion, pHLIP*d*-Eto, regarding the three parameters previously described are depicted in Table 2. Of note, the *pKa* values of 6.25 are in the same range as the pH_e observed in the tumor microenvironment (~pH 6.5) and much higher than those obtained for pHLIP*d*. The difference of *pKa* values (Table 2) between pHLIP*d* and pHLIP*d*-Eto indicates that the addition of etomoxir increased the peptide hydrophobicity and thus its affinity for the membrane.

Table 2
Comparison of pKa of two published pHLIPs (Var3 (Weerakkody, Moshnikova et al. 2013)**, pHLIP*r*** (Scott, Westerfield et al. 2017)**), pHLIP*d* and pHLIP*d*-Eto.** The determination of pKa values was based on the fluorescence spectrum regarding the center of mass (CM), the maximum spectral (SM), and the fluorescence intensity at 335 nm (FI_{335}). The pKa corresponds to pH in which 50% peptide is inserted in liposomes. For pHLIP*d*-Eto, the values were approximately 6.0. *Values found in the literature.

	SM		CM		FI_{335}	
	pKa		*pKa*		*pKa*	
Var3*	5.06					
pHLIP*r**	6.22 (±0.17)		6.07 (±0.08)		5.68 (±0.09)	
N = 2	***pKa***	**95%CI**	***pKa***	**95%CI**	***pKa***	**95%CI**
pHLIP*d*	4.95	4.80–5.11	4.97	4.84 – 5.09	4.78	4.69 – 4.88
pHLIP*r*	6.25	5.72–6.78	5.97	5.78 – 6.06	6.16	5.67 – 6.65
pHLIP*d*-Eto	6.29	6.19 – 6.46	6.41	6.04 – 6.46	6.10	6.02 – 6.19

3.4. Pilot in vitro evaluation of conjugates

POPC vesicles are a straightforward model for investigating membrane insertion of peptides but do not represent the complexity of a cell membrane (Szlasa, Zendran et al. 2020). The affinity of a peptide for vesicles and its insertion actually vary according to the nature of lipids and the presence of cholesterol (Barrera, Fendos et al. 2012, Kyrychenko, Vasquez-Montes et al. 2015, Vasquez-Montes, Gerhart et al. 2018). Therefore, we next decided to work on a *in cellulo* model in order to check the delivery of the drug. Moreover, as previously documented (Dierge, Debock et al. 2021), we also included culture conditions where docosahexaenoic acid (DHA) was added in the extracellular medium to

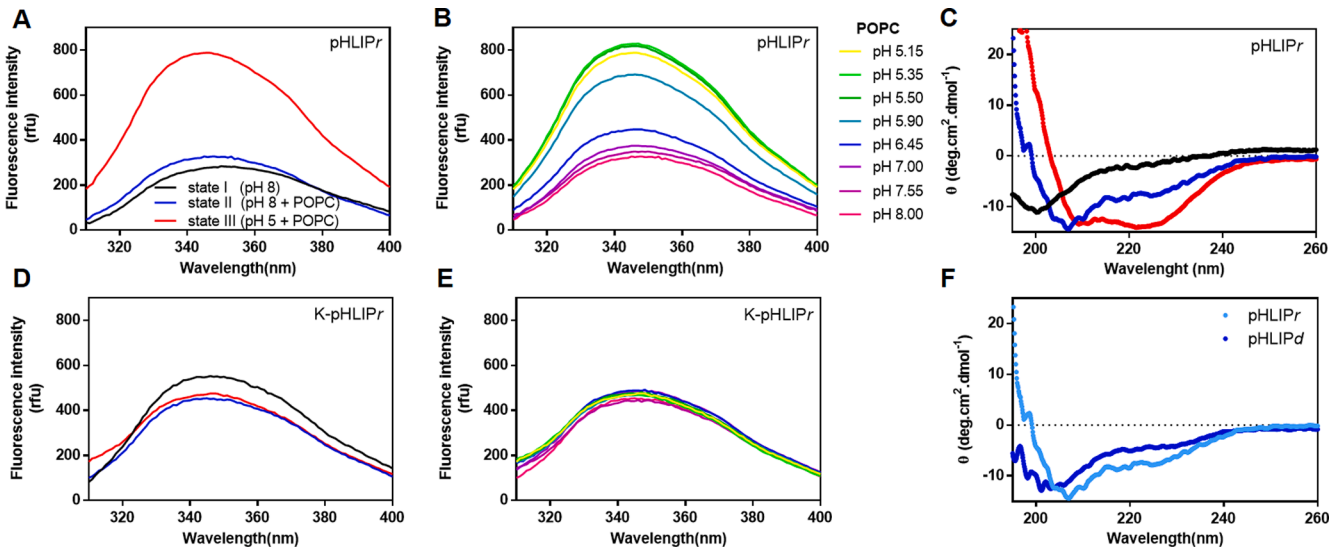


Fig. 5. Interactions of published peptide (pHLIP*r*) and its negative control (K-pHLIP*r*) with lipid bilayers. Tryptophan fluorescence measurements (**A, B, D, E**) and CD spectroscopy (**C**) of peptides in state I (pH 8), state II (pH 8 and POPC vesicles), and state III (pH 5 and POPC vesicles). pHLIP*r* presents a pH-dependent insertion (**A,B**) and structuration (**C**) inside the POPC vesicles, while K-pHLIP*r* shows no preference (**D, E**) at various pH conditions. Overlay of state II CD spectra for pHLIP*d* and pHLIP*r* (**F**) shows that pHLIP*d* is less structured than pHLIP*r* in alkaline conditions with lipid bilayers.

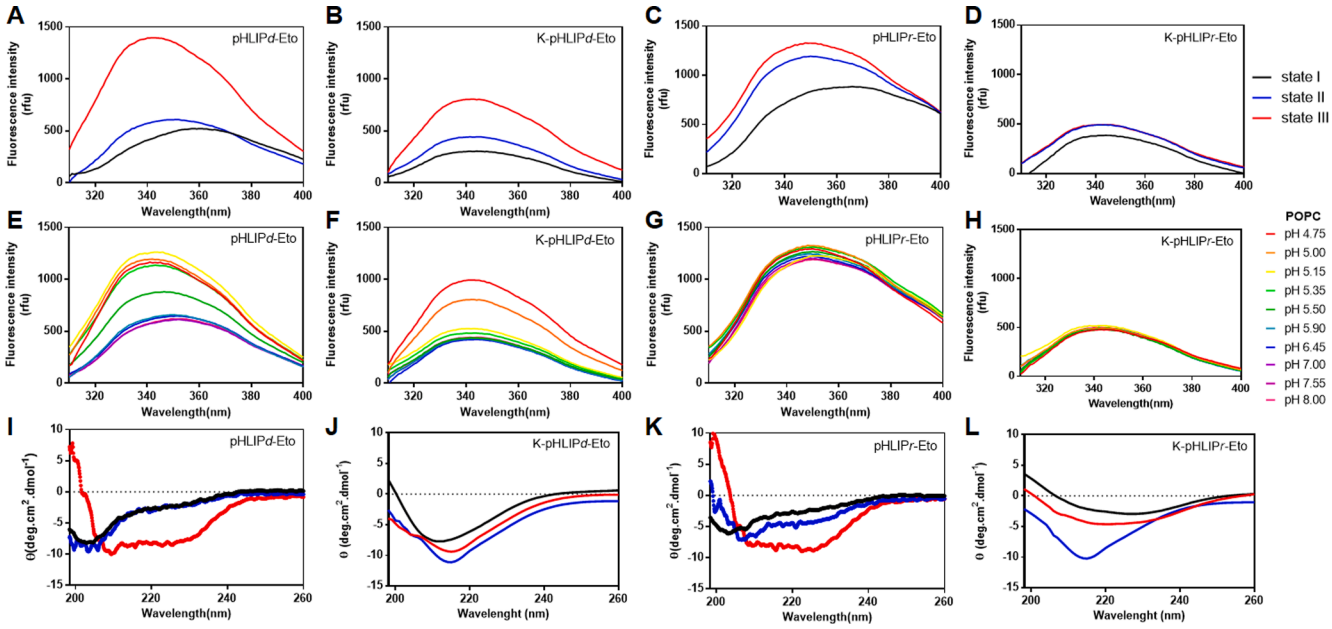


Fig. 6. Interactions of conjugates (pHLIP*d*/*r*-Eto) and their negative controls (K-pHLIP*d*/*r*-Eto) with lipid bilayer. Tryptophan fluorescence measurements (**A-H**) and CD spectroscopy (**I-L**) of peptides in state I (pH 8), state II (pH 8 and POPC vesicles) and state III (pH 5 and POPC vesicles). Only pHLIP*d*-Eto behaves strictly like a peptide of pHLIP family; the medium acidity provokes its insertion (**A, E**) and structuration (**I**) in the presence of a lipid bilayer. pHLIP*r*-Eto, K-pHLIP*r*-Eto and K-pHLIP*d*-Eto display less preference on their insertion (**B-D, F-H**) and structuration (**J-L**) properties in presence of the liposomes.

sensitize acidic cancer cells to ferroptosis.

To assess the ability of the conjugates to target acidic cancer cells and induce an equivalent toxicity as Eto alone, the human epithelial cell line FaDu, derived from a squamous cell carcinoma of the hypopharynx, maintained under neutral pH conditions (7.4/FaDu) or pre-adapted to an acidic pH (6.5/FaDu) was treated with 10 μM Eto or the conjugates. Both pHLIP*d*-Eto and pHLIP*r*-Eto induced a decrease in cell density of DHA-exposed 6.5/FaDu cancer cells *i.e.* to the same extent as Eto alone (Fig. 7 **B**). Importantly, 7.4/cancer cells did not reveal signs of toxicity when exposed to either conjugate (or Eto) in the presence of DHA (Fig. 7 **B**).

4. Discussion

Previous studies showed that pHLIP linked to small fluorophores or imaging agent selectively target acidic cancer cells (Andreev, Dupuy et al. 2007, Reshetnyak, Yao et al. 2011, Weerakkody, Moshnikova et al. 2013, Adochite, Moshnikova et al. 2014, Tapmeier, Moshnikova et al. 2015, Adochite, Moshnikova et al. 2016). Polar cytotoxic molecules conjugated to pHLIP presented a better selectivity for acidic tumor cells than their free version (An, Wijesinghe et al. 2010, Song, Chuan et al. 2016). Also, some conjugates display better tumor-targeting than pHLIP with no cargo (Svoronos, Bahal et al. 2020). Cargo polarity plays an important role in the affinity of a conjugate for a lipid bilayer; anticancer

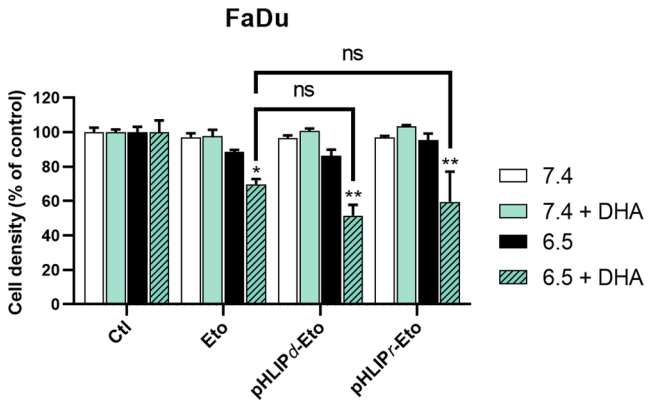


Fig. 7. Etomoxir linked to pHLIP*d* and pHLIP*r* increases DHA toxicity in acid-adapted cancer cells. Effects of 10 μM etomoxir (Eto), pHLIP*d*-etomoxir (pHLIP*d*-Eto) and pHLIP*r*-etomoxir (pHLIP*r*-Eto) on 2D FaDu cancer cells exposed to 100 μM of docosahexaenoic acid (DHA). Data are represented as mean ± SEM of 6 different wells. Significance for the effects of etomoxir was determined by two-way ANOVA with Sidak's multiple comparison *p < 0.05; **p < 0.01.

agents with log P of ~ −3 and molecular weights of ~ 800 g/mol were found to be efficiently delivered into cancer cells (Thévenin, An et al. 2009). Moreover, lipid composition and membrane physical properties have been previously shown to impact pHLIP transmembrane insertion. (Barrera, Fendos et al. 2012, Kyrychenko, Vasquez-Montes et al. 2015, Vasquez-Montes, Gerhart et al. 2018) To our knowledge, no potential anticancer agents with a log P higher than 2.2 was conjugated to a pHLIP (Burns, Robinson et al. 2015).

Etomoxir is a well-known inhibitor of CPT1, a validated target for anticancer therapy. This drug conforms to Lipinski rule of 5 (Mw: 298.76 g/mol, Log P: 3.9, no hydrogen bond donor, 4 hydrogen bond acceptors) and is characterized by an adequate polar surface area (PSA) to ensure membrane permeability (61.9 $Å^2$). Eto is however known to be hepatotoxic (Holubarsch, Rohrbach et al. 2007) which prevents its broader use. Our aim was thus to design a new pHLIP-conjugate of Eto to generate a safer drug. We successfully conjugated Eto to (K)-pHLIPs following the procedure already described for other conjugates. Intrinsic tryptophan fluorescence and CD experiments revealed a pH-dependent folding of pHLIP*d*-Eto as anticipated for a pHLIP conjugate (*i.e.* a structuration followed by insertion inside POPC vesicles). On the contrary, our data suggest that pHLIP*r*-Eto does not exhibit a preference for any of the pH-conditions tested. Hence, it appears that this conjugate is slightly structured at basic condition in presence of POPC vesicles which might explain the non-preference of pH. Hence, our results suggest that pHLIP*r* sequence is too hydrophobic for conjugating a drug with an already high lipophilicity (logP < 2.2) to observe a pH-preference for membrane insertion. As seen from the CD spectra, negative controls of these conjugates aggregate due to the positive charges on the peptide at physiological pH. Both synthetized conjugates however decrease the growth of acidic cancer cells (pre-challenged with DHA). As no effects in 7.4/cancer cells were observed, the insertion of pHLIP-Eto conjugates is dependent of the medium pH. Further, for the etomoxir conjugation, the proportion of polar residues in the sequence impacts conjugate insertion as the sequence with the more polar residues present a better insertion in acidic cancer cells. The next step will be to test etomoxir conjugates *in vivo* to hopefully confirm anticancer effects while sparing healthy tissues and particularly the liver.

In conclusion, our results demonstrate that pHLIP technology can be successfully applied to apolar anticancer cargoes. Our work suggests that peptide insertion depends on the lipid composition but also on the peptide sequence and cargo polarity.

CRediT authorship contribution statement

Marine Deskeuvre: Conceptualization, Writing – review & editing. **Junjie Lan:** . **Emeline Dierge:** . **Joris Messens:** Writing – review & editing, Resources. **Olivier Riant:** Resources. **Cyril Corbet:** Writing – review & editing. **Olivier Feron:** Conceptualization, Writing – review & editing, Resources, Supervision. **Raphaël Frédérick:** Conceptualization, Writing – review & editing, Resources, Supervision.

Declaration of Competing Interest

The authors declare that they have no known competing financial interests or personal relationships that could have appeared to influence the work reported in this paper.

Data availability

Data will be made available on request.

Acknowledgments

This work was supported by the Université Catholique de Louvain, Belgium. The authors thank Vincent Stroobant, Bénédicte Tollet, Bernard Ukacar, Kevin Vanvarenberg, Khadija Wahni and Santiago Agustín Martínez Gache for technical assistance and fruitful discussions. We acknowledge the VIB-VUB Center for Structural Biology for access to the circular dichroism instrument and Pr. Rita Vanbever (UCLouvain) for the access to Avanti Mini Extruder.

Appendix A. Supplementary data

Supplementary data to this article can be found online at https://doi.org/10.1016/j.ijpharm.2022.122041.

References

Adochite, R.-C., Moshnikova, A., Carlin, S.D., Guerrieri, R.A., Andreev, O.A., Lewis, J.S., Reshetnyak, Y.K., 2014. Targeting breast tumors with pH (low) insertion peptides. Mol. Pharm. 11 (8), 2896–2905.
Adochite, R.C., Moshnikova, A., Golijanin, J., Andreev, O.A., Katenka, N.V., Reshetnyak, Y.K., 2016. Comparative Study of Tumor Targeting and Biodistribution of pH (Low) Insertion Peptides (pHLIP((R)) Peptides) Conjugated with Different Fluorescent Dyes. Mol Imaging Biol 18 (5), 686–696.
An, M., Wijesinghe, D., Andreev, O.A., Reshetnyak, Y.K., Engelman, D.M., 2010. pH-(low)-insertion-peptide (pHLIP) translocation of membrane impermeable phalloidin toxin inhibits cancer cell proliferation. Proc. Natl. Acad Sci. USA 107 (47), 20246–20250.
Andreev, O.A., Dupuy, A.D., Segala, M., Sandugu, S., Serra, D.A., Chichester, C.O., Engelman, D.M., Reshetnyak, Y.K., 2007. Mechanism and uses of a membrane peptide that targets tumors and other acidic tissues in vivo. Proc. Natl. Acad Sci. USA 104 (19), 7893–7898.
Anschau, A., Caruso, C.S., Kuhn, R.C., Franco, T.T., 2017. Validation of the sulfo-phosphovanillin (SPV) method for the determination of lipid content in oleaginous microorganisms. Braz. J. Chem. Eng. 34 (1), 19–27.
Barrera, F.N., Fendos, J., Engelman, D.M., 2012. Membrane physical properties influence transmembrane helix formation. Proc Natl Acad Sci U S A 109 (36), 14422–14427.
Burns, K.E., Robinson, M.K., Thévenin, D., 2015. Inhibition of cancer cell proliferation and breast tumor targeting of pHLIP-monomethyl auristatin E conjugates. Mol. Pharm. 12 (4), 1250–1258.
Burns, K.E., McCleerey, T.P., Thevenin, D., 2016. pH-Selective Cytotoxicity of pHLIP-Antimicrobial Peptide Conjugates. Sci. Rep. 6, 28465.
Burns, K.E., Hensley, H., Robinson, M.K., Thévenin, D., 2017. Therapeutic Efficacy of a Family of pHLIP-MMAF Conjugates in Cancer Cells and Mouse Models. Mol. Pharm. 14 (2), 415–422.
Carracedo, A., Cantley, L.C., Pandolfi, P.P., 2013. Cancer metabolism: fatty acid oxidation in the limelight. Nat. Rev. Cancer 13 (4), 227–232.
Cheng, C.J., Bahal, R., Babar, I.A., Pincus, Z., Barrera, F., Liu, C., Svoronos, A., Braddock, D.T., Glazer, P.M., Engelman, D.M., Saltzman, W.M., Slack, F.J., 2015. MicroRNA silencing for cancer therapy targeted to the tumour microenvironment. Nature 518 (7537), 107–110.
Corbet, C., Draoui, N., Polet, F., Pinto, A., Drozak, X., Riant, O., Feron, O., 2014. The SIRT1/HIF2alpha axis drives reductive glutamine metabolism under chronic acidosis and alters tumor response to therapy. Cancer Res. 74 (19), 5507–5519.
Corbet, C., Bastien, E., Santiago de Jesus, J.P., Dierge, E., Martherus, R., Vander Linden, C., Doix, B., Degavre, C., Guilbaud, C., Petit, L., Michiels, C., Dessy, C.,

Larondelle, Y., Feron, O., 2020. TGFbeta2-induced formation of lipid droplets supports acidosis-driven EMT and the metastatic spreading of cancer cells. Nat. Commun. 11 (1), 454–469.
Corbet, C., Feron, O., 2017a. Emerging roles of lipid metabolism in cancer progression. Curr Opin Clin Nutr Metab Care 20 (4), 254–260.
Corbet, C., Feron, O., 2017b. Tumour acidosis: from the passenger to the driver's seat. Nat. Rev. Cancer 17 (10), 577–593.
Corbet, C., Pinto, A., Martherus, R., Santiago de Jesus, J., Polet, F., Feron, O., 2016. Acidosis Drives the Reprogramming of Fatty Acid Metabolism in Cancer Cells through Changes in Mitochondrial and Histone Acetylation. Cell Metab. 24 (2), 311–323.
Deep, G., Schlaepfer, I.R., 2016. Aberrant Lipid Metabolism Promotes Prostate Cancer: Role in Cell Survival under Hypoxia and Extracellular Vesicles Biogenesis. Int. J. Mol. Sci. 17 (7), 1061–1075.
Dierge, E., Debock, E., Guilbaud, C., Corbet, C., Mignolet, E., Mignard, L., Bastien, E., Dessy, C., Larondelle, Y., Feron, O., 2021. Peroxidation of n-3 and n-6 polyunsaturated fatty acids in the acidic tumor environment leads to ferroptosis-mediated anticancer effects. Cell Metab. 33 (8), 1701–1715.e5.
Gärtner, D., Stein, A.L., Grupe, S., Arp, J., JacobivonWangelin, A., 2015. Iron-Catalyzed Cross-Coupling of Alkenyl Acetates. Angew. Chem. Int. Ed. Engl. 54 (36), 10545–10549.
Gayle, S., Aiello, R., Leelatian, N., Beckta, J.M., Bechtold, J., Bourassa, P., Csengery, J., Maguire, R.J., Marshall, D., Sundaram, R.K., Van Doorn, J., Jones, K., Moore, H., Lopresti-Morrow, L., Paradis, T., Tylaska, L., Zhang, Q., Visca, H., Reshetnyak, Y.K., Andreev, O.A., Engelman, D.M., Glazer, P.M., Bindra, R.S., Paralkar, V.M., 2021. Tumor-selective, antigen-independent delivery of a pH sensitive peptide-topoisomerase inhibitor conjugate suppresses tumor growth without systemic toxicity. NAR Cancer 3 (2), 1–13.
Holubarsch, C.J., Rohrbach, M., Karrasch, M., Boehm, E., Polonski, L., Ponikowski, P., Rhein, S., 2007. A double-blind randomized multicentre clinical trial to evaluate the efficacy and safety of two doses of etomoxir in comparison with placebo in patients with moderate congestive heart failure: the ERGO (etomoxir for the recovery of glucose oxidation) study. Clin Sci (Lond) 113 (4), 205–212.
Horikawa, R., Sunayama, H., Kitayama, Y., Takano, E., Takeuchi, T., 2016. A Programmable Signaling Molecular Recognition Nanocavity Prepared by Molecular Imprinting and Post-Imprinting Modifications. Angew. Chem. Int. Ed. Engl. 55 (42), 13023–13027.
Kang, G., Yamagami, M., Vellalath, S., Romo, D., 2018. Enantioselective Synthesis of Medium-Sized Lactams via Chiral alpha, beta-Unsaturated Acylammonium Salts. Angew. Chem. Int. Ed. Engl. 57 (22), 6527–6531.
Kyrychenko, A., Vasquez-Montes, V., Ulmschneider, M., Ladokhin, A., 2015. Lipid headgroups modulate membrane insertion of pHLIP peptide. Biophys. J . 108 (4), 791–794.
Moshnikova, A., Moshnikova, V., Andreev, O.A., Reshetnyak, Y.K., 2013. Antiproliferative effect of pHLIP-amanitin. Biochemistry 52 (7), 1171–1178.
Onyango, J.O., Chung, M.S., Eng, C.-H., Klees, L.M., Langenbacher, R., Yao, L., An, M., 2015. Noncanonical amino acids to improve the pH response of pHLIP insertion at tumor acidity. Angew. Chem. Int. Ed. Engl. 54 (12), 3658–3663.
Peppicelli, S., Andreucci, E., Ruzzolini, J., Laurenzana, A., Margheri, F., Fibbi, G., Del Rosso, M., Bianchini, F., Calorini, L., 2017. The acidic microenvironment as a possible niche of dormant tumor cells. Cell. Mol. Life Sci. 74 (15), 2761–2771.
Pillai, S.R., Damaghi, M., Marunaka, Y., Spugnini, E.P., Fais, S., Gillies, R.J., 2019. Causes, consequences, and therapy of tumors acidosis. Cancer Metastasis Rev. 38 (1–2), 205–222.
Reshetnyak, Y.K., Andreev, O.A., Lehnert, U., Engelman, D.M., 2006. Translocation of molecules into cells by pH-dependent insertion of a transmembrane helix. Proc Natl Acad Sci U S A 103 (17), 6460–6465.
Reshetnyak, Y.K., Segala, M., Andreev, O.A., Engelman, D.M., 2007. A monomeric membrane peptide that lives in three worlds: in solution, attached to, and inserted across lipid bilayers. Biophys. J. 93 (7), 2363–2372.
Reshetnyak, Y.K., Yao, L., Zheng, S., Kuznetsov, S., Engelman, D.M., Andreev, O.A., 2011. Measuring tumor aggressiveness and targeting metastatic lesions with fluorescent pHLIP. Mol Imaging Biol 13 (6), 1146–1156.
Sawyer, B. T., L. Qamar, T. M. Yamamoto, A. McMellen, Z. L. Watson, J. K. Richer, K. Behbakht, I. R. Schlaepfer and B. G. Bitler (2020). "Targeting Fatty Acid Oxidation to Promote Anoikis and Inhibit Ovarian Cancer Progression." Mol Cancer Res **18**(7): 1088-1098.
Schlaepfer, I. R., L. Rider, L. U. Rodrigues, M. A. Gijon, C. T. Pac, L. Romero, A. Cimic, S. J. Sirintrapun, L. M. Glode, R. H. Eckel and S. D. Cramer (2014). "Lipid catabolism via CPT1 as a therapeutic target for prostate cancer." Mol Cancer Ther **13**(10): 2361-2371.
Scott, H.L., Westerfield, J.M., Barrera, F.N., 2017. Determination of the Membrane Translocation pK of the pH-Low Insertion Peptide. Biophys. J . 113 (4), 869–879.
Song, Q., Chuan, X., Chen, B., He, B., Zhang, H., Dai, W., Wang, X., Zhang, Q., 2016. A smart tumor targeting peptide-drug conjugate, pHLIP-SS-DOX: synthesis and cellular uptake on MCF-7 and MCF-7/Adr cells. Drug Deliv 23 (5), 1734–1746.
Svoronos, A.A., Bahal, R., Pereira, M.C., Barrera, F.N., Deacon, J.C., Bosenberg, M., DiMaio, D., Glazer, P.M., Engelman, D.M., 2020. Tumor-Targeted, Cytoplasmic Delivery of Large, Polar Molecules Using a pH-Low Insertion Peptide. Mol. Pharm. 17 (2), 461–471.
Szlasa, W., Zendran, I., Zalesińska, A., Tarek, M., Kulbacka, J., 2020. Lipid composition of the cancer cell membrane. J. Bioenerg. Biomembr. 52 (5), 321–342.
Tapmeier, T.T., Moshnikova, A., Beech, J., Allen, D., Kinchesh, P., Smart, S., Harris, A., McIntyre, A., Engelman, D.M., Andreev, O.A., Reshetnyak, Y.K., Muschel, R.J., 2015. The pH low insertion peptide pHLIP Variant 3 as a novel marker of acidic malignant lesions. Proc Natl Acad Sci U S A 112 (31), 9710–9715.
Thévenin, D., An, M., Engelman, D.M., 2009. pHLIP-mediated translocation of membrane-impermeable molecules into cells. Chem. Biol. 16 (7), 754–762.
Vander Linden, C., Corbet, C., 2019. Therapeutic Targeting of Cancer Stem Cells: Integrating and Exploiting the Acidic Niche. Front. Oncol. 9, 159.
Vasquez-Montes, V., Gerhart, J., King, K.E., Thévenin, D., Ladokhin, A.S., 2018. Comparison of lipid-dependent bilayer insertion of pHLIP and its P20G variant. Biochim. Biophys. Acta, Biomembr. 1860 (2), 534–543.
Wang, Y.-N., Zeng, Z.-L., Lu, J., Wang, Y., Liu, Z.-X., He, M.-M., Zhao, Q.i., Wang, Z.-X., Li, T., Lu, Y.-X., Wu, Q.-N., Yu, K., Wang, F., Pu, H.-Y., Li, B.o., Jia, W.-H., shi, M., Xie, D., Kang, T.-B., Huang, P., Ju, H.-Q., Xu, R.-H., 2018. CPT1A-mediated fatty acid oxidation promotes colorectal cancer cell metastasis by inhibiting anoikis. Oncogene 37 (46), 6025–6040.
Weerakkody, D., Moshnikova, A., Thakur, M.S., Moshnikova, V., Daniels, J., Engelman, D.M., Andreev, O.A., Reshetnyak, Y.K., 2013. Family of pH (low) insertion peptides for tumor targeting. Proc Natl Acad Sci U S A 110 (15), 5834–5839.
Wijesinghe, D., Engelman, D.M., Andreev, O.A., Reshetnyak, Y.K., 2011. Tuning a polar molecule for selective cytoplasmic delivery by a pH (Low) insertion peptide. Biochemistry 50 (47), 10215–10222.